SUBGRID-SCALE ENSTROPHY TRANSFER IN TURBULENT WALL BOUNDED FLOWS

G. Hauët
Instituto Superior Técnico, Pav. Mecânica I, 1^o andar/LASEF,
Av. Rovisco Pais, 1049-001, Lisboa, Portugal
hauet@ist.utl.pt

C. B. da Silva
Instituto Superior Técnico, Pav. Mecânica I, 1^o andar/LASEF,
Av. Rovisco Pais, 1049-001, Lisboa, Portugal
carlos.silva@ist.utl.pt

J. C. F. Pereira
Instituto Superior Técnico, Pav. Mecânica I, 1^o andar/LASEF,
Av. Rovisco Pais, 1049-001, Lisboa, Portugal
pereira@ist.utl.pt

ABSTRACT

A-priori **tests are carried out to analyse the SGS enstrophy transfer in turbulent channel flow. The SGS enstrophy transfer is negative (SGS enstrophy backscatter) in the viscous sublayer until $y^+ \simeq 6$, where it becomes positive (SGS enstrophy forward scatter). The maximum enstrophy dissipation is found to be located at about 8 wall units, where a strong correlation is detected between the high-speed streaks and the SGS enstrophy dissipation.**

INTRODUCTION

One of the most important challenges faced by large-eddy simulations (LES) concerns the reproduction of the near wall physics on meshes coarser than the ones used in direct numerical simulations (DNS). An ideal situation would be to place the first grid point within the buffer layer ($y^+ \approx 5 - 30$), without prescribing a wall law. However, the physics of the buffer layer play a crucial role in determining the correct turbulent statistics. In particular, it is well known that the quasi-streamwise vortices from the inner layer have to be well captured (Jiménez and Moin, 1991).

An important and related issue concerns the role played by the subgrid-scale (SGS) models on the vortices obtained in LES, which was analysed recently in turbulent plane jets by da Silva and Pereira (2004). Using DNS and LES of turbulent plane jets they showed that the key for understanding the effect of SGS models on the vortices computed from LES is the analysis of the resolved or grid scale enstrophy transport equation:

$$
\begin{aligned}
\frac{D\left(\frac{1}{2}\widetilde{\Omega}_i\widetilde{\Omega}_i\right)}{Dt} = \quad & \widetilde{\Omega}_i\widetilde{\Omega}_j\widetilde{S}_{ij} + \nu\frac{\partial^2\left(\frac{1}{2}\widetilde{\Omega}_i\widetilde{\Omega}_i\right)}{\partial x_i \partial x_j} \\
- \quad & \nu\frac{\partial\widetilde{\Omega}_i}{\partial x_j}\frac{\partial\widetilde{\Omega}_i}{\partial x_j} - \epsilon_{ijk}\widetilde{\Omega}_i\frac{\partial^2\tau_{kp}}{\partial x_j \partial x_p}
\end{aligned}
$$

where $\tau_{ij} = \widetilde{u_i u_j} - \widetilde{u}_i\widetilde{u}_j$ is the subgrid stress tensor, and $\widetilde{\Omega}_i$ denotes the filtered or resolved vorticity.

Since the vortices are regions of concentrated enstrophy, the effect of the SGS models on these structures is given by the last term in the above equation: the SGS ENSTROPHY DISSIPATION. In LES of isotropic turbulence or in turbulent jets this term is (on average) negative, and represents the dissipation of enstrophy caused by the particular SGS model used.

The goal of the present work is to extend the analysis of da Silva and Pereira (2004) to the more difficult and important context of wall flows.

TURBULENT CHANNEL FLOW DNS

For this purpose we carried out DNS of a turbulent channel flow with Reynolds number equal to $Re_\tau = u_\tau\delta/\nu = 180$, where u_τ is the friction velocity and δ is the channel half-height. The computational domain extends to $4\pi\delta \times 2\delta \times 4\pi\delta/3$ along the streamwise (x), normal (y), and spanwise (z) directions respectively, as in Kim *et al.* (1987), and the resolution is $192 \times 151 \times 128$ grid points along these directions which gives a mesh spacing equal to $\Delta_x^+ \times \Delta_y^+|_{wall}/\Delta_y^+|_{center} \times \Delta_z^+ = 11.84 \times 0.56/4.38 \times 5.87$.

The numerical code used in the present simulations is a classical staggered finite difference Navier-Stokes solver using a centred second order scheme for spatial discretizations and a third order Runge-Kutta scheme for temporal advancement. The pressure-velocity coupling is achieved by a fractional step method, where a Poisson equation is solved using spectral schemes in the homogeneous directions and a tridiagonal matrix solver in the wall normal direction. Full details are given in Orlandi (2000).

The separation between grid and subgrid-scales was made with the 3D box filters. The filter widths tested are equal to $\overline{\Delta_x}/\Delta_x = \overline{\Delta_z}/\Delta_z = 2$ and 6, a further filtering is applied along the wall normal direction $\overline{\Delta_y}(y^+)/\Delta_y(y^+) = 2$ and 6.

RESULTS

Validation

Figure 1 shows the mean streamwise velocity profile of the present DNS compared to the wall laws in a channel flow: $U = y$ and $U = 2.47ln(y) + 5.5$. Figure 2 shows the root mean square of vorticity fluctuations compared with the DNS results of del Alamo *et. al* (2005). As can be seen the present DNS agrees very well with the other references. The same is true of the rms velocity profiles (see Hauët *et. al*, 2007).

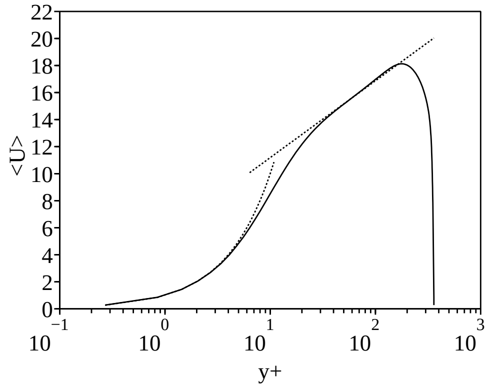

Figure 1: Mean profile of the streamwise velocity in wall units (solid line). $U = y$ and $U = 2.47ln(y) + 5.5$ (dashed lines).

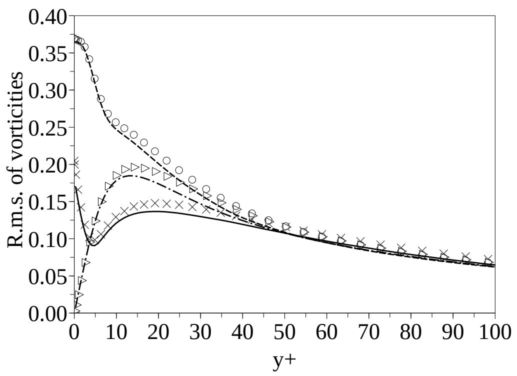

Figure 2: Profiles of root-mean-square vorticity in the present DNS (lines) and from the DNS of del Alamo *et al.* (2005, symbols). —— , ×: Ω'_x, $\cdots$, △ : Ω'_y, – – , o : Ω'_z.

A priori tests: the SGS enstrophy dissipation

Figure 3 shows mean profiles of SGS enstrophy dissipation divided into its total, mean and fluctuating contributions for two 3D box filters (with $\Delta/\Delta_x = 2, 6$). The symbols are for the smallest filter. In the viscous sublayer, the three components are close to zero. The profile for the 3D box filter with $\Delta/\Delta x = 6$ are the solid, dashed and dotted lines. The first four points at the wall are not shown due to the lower order accuracy of the boundary conditions. Small and large filters display the same behaviour of the SGS enstrophy dissipation. At $y^+ \simeq 3$ and $y^+ \simeq 10$, two extrema are found in both cases. As the distance from the wall increases the SGS enstrophy dissipation attains a small negative value (meaning enstrophy forward scatter), and by

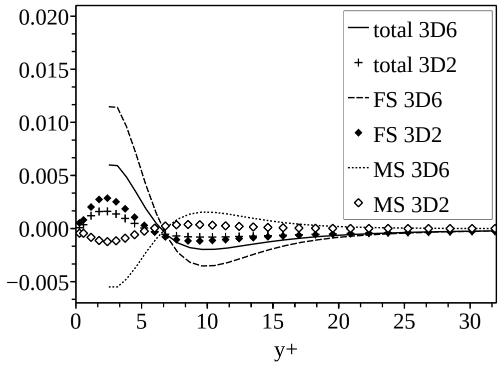

Figure 3: Zoom in the buffer layer of the mean profiles of Total SGS enstrophy transfer, SGS enstrophy transfer due to the mean flow MS and due to the turbulent fluctuations FS (all profiles in wall units) with two different sizes of the 3D box filter.

$y^+ \approx 30$, this value is more or less constant, as occurs in isotropic turbulence or in turbulent plane jets (da Silva and Pereira, 2004). However, as one approaches the wall the total SGS enstrophy dissipation decreases attaining a minimum, well within the buffer layer (at about $y^+ = 14$). In order to explain this result the SGS enstrophy dissipation is divided into a mean and fluctuating part:

$$-\epsilon_{ijk} < \widetilde{\Omega}_i \frac{\partial^2 \tau_{kp}}{\partial x_j \partial x_p} > = - \epsilon_{ijk} < \widetilde{\Omega}_i >< \frac{\partial^2 \tau_{kp}}{\partial x_j \partial x_p} > - \epsilon_{ijk} < \widetilde{\Omega}'_i \frac{\partial^2 \tau'_{kp}}{\partial x_j \partial x_p} >$$

In the viscous sublayer, in strong contrast to isotropic turbulence or turbulence at the far field of a turbulent jet, two new facets emerge: (a) there is a marked influence of the mean field gradient on the overall SGS enstrophy transfer, as can be seen by the non negligible value taken by its mean contribution and; (b) the SGS enstrophy dissipation exhibits a mean backscatter (backward enstrophy transfer) contribution. Notice that the value of the fluctuating part is two times the mean contribution. The switch between source and dissipation of the SGS enstrophy occurs at $y^+ \simeq 6$ and is independent of the size of the box filter. Other tests with 2D box filters (not shown) confirm these results.

Impact of the enstrophy dissipation on the high/low speed streaks

In order to see whether it is possible to link the above results to the deterministic structures present in wall flows, as described in detail in *e.g* Robinson (1991), several visualisations and turbulent statistics were analysed in the buffer layer. The most interesting results concern the existence of a clear link between the SGS enstrophy dissipation and the regions of high speed streaks. Profiles of the correlation coefficient between these variables (fig. 4) display a maximum of about 20% and 45%, respectively, at about $y^+ \simeq 7$ for the both size filters 2 and 6, and decreases very fast both when approaching the wall and when approaching the centre of the channel, where this correlation coefficient is negligible. For the smallest filter, the correlation coefficient between the streamwise velocity and the enstrophy dissipation is negligible.

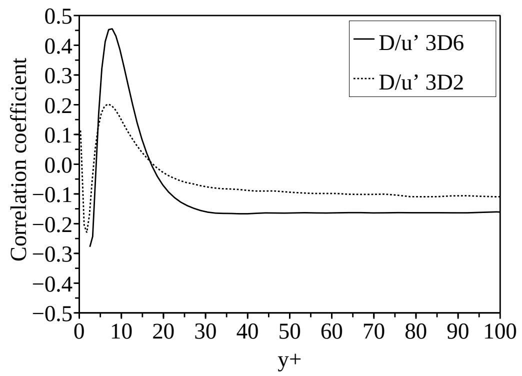

Figure 4: Correlation coefficient of the streamwise velocity fluctuation and the SGS enstrophy dissipation along the channel height for 3D box filter with $\Delta/\Delta x = 2$ and 6 (dotted and solid lines respectively).

A spatial coincidence between low-speed streaks (LSS) and regions of strong energy backscatter at $y^+ \approx 2.8$ was observed by Schlatter *et al.* (2005). For the biggest filter we found a slight spatial correlation between the low-speed streaks (LSS) and the enstrophy inverse cascade (see Hauët *et al.*, 2007). To confirm the spatial coincidence, conditional averages, similar to the ones of Piomelli *et al.* (1996) were made in the channel flow, but focusing on the SGS enstrophy instead of the SGS energy transfer. A normal slice at $y^+ \simeq 7$ of the conditionally-averaged field is shown in Fig. 5. This field was obtained using all the 100 instantaneous fields from the present data bank where about 1400 energy forward scatter events were detected at $y^+ = 14$. The most intense regions of positive values of streamwise velocity and forward scatter enstrophy (negative values) occur at the same location. This indicates that the dominating structures from the buffer layer obtained from large-eddy simulations, *i.e.* the quasi-streamwise vortices, are to be mainly dissipated at the high speed streaks region.

Dissipation on the quasi-streamwise vortices in the buffer layer

In order to assess the SGS enstrophy dissipation on the vortices, we propose to analyse the previous conditionally-averaged field of the Q-criterium (Dubief and Delcayre, 2000). Q is defined by $\frac{1}{2}(\Omega_{ij}\Omega_{ij} - S_{ij}S_{ij})$, where Ω_{ij} and S_{ij} are respectively the antisymmetrical and symmetrical part of the velocity gradient tensor $A_{ij} = \partial_j u_i$. Fig. 6 shows a spanwise slice of the conditionally-averaged field of Q-criterium and SGS enstrophy transfer. The negative values of Q, where the strain dominates, are mainly at the same location of the SGS enstrophy forward scatter events. Piomelli *et. al*(1996) show that strong shear layers can be linked with SGS energy forward scatter also. The SGS enstrophy dissipation is maximum where the quasi-streamwise vortices are detached from the wall, i.e. where the "legs" of the hairpin vortex raise from the wall to become the head of the vortex (see Robinson, 1991).

CONCLUSIONS

High-speed streaks in a low Reynolds number channel flow are strongly correlated with the SGS enstrophy forward scatter, as confirmed by instantaneous visualisations, correlations and conditional averaging. The maximum dissipation of the wall vortices occurs around the head of the

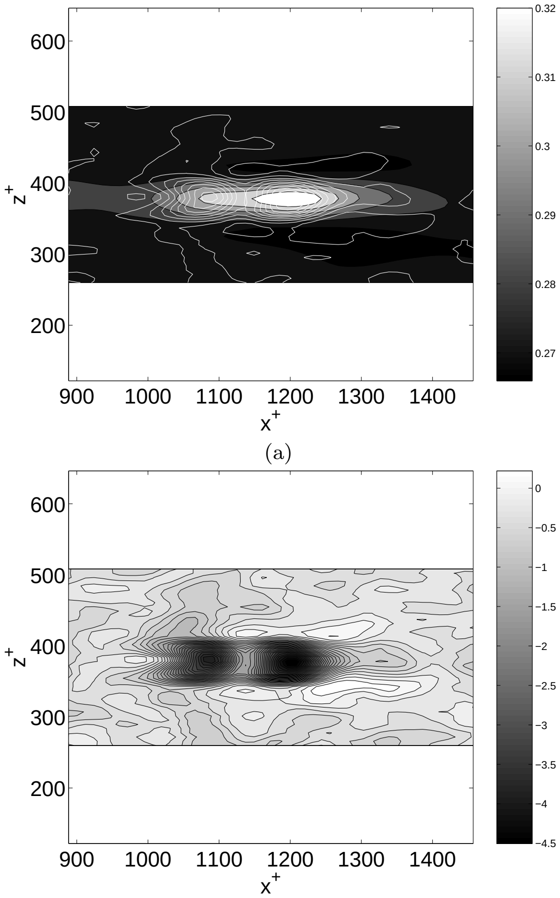

(b)

Figure 5: Forward scatter event of SGS energy dissipation detected at $y^+ \simeq 14$. (a) Map of streamwise velocity and (white) contours of SGS enstrophy dissipation at $y^+ \simeq 7$. (b) Map of SGS enstrophy dissipation. All values are in global units.

hairpin vortices in the region of strong shear. Ongoing work is aimed at analysing the performance of several SGS models in reproducing the high/low speed streaks and the vortices from the buffer layer. More details can be found in Hauët *et al.* (2007).

REFERENCES

da Silva, C. B. and Pereira, J. C. F., 2004, "The effect of subgrid-scale models on the vortices computed from large-eddy simulations", Phys. Fluids, Vol. 16, Num. 12, pp. 4506.

Dubief, Y. and Delcayre, F., 2000, "On coherent-vortex identification in turbulence", J. of Turbulence, Vol. 1.

Hauët, G., da Silva, C. B. and Pereira, J. C. F., 2007, "The effect of subgrid-scale models on the near wall vortices: *a-priori* tests", Phys. Fluids, *in press*.

Jiménez, J. and Moin, P., 1991, "The minimal flow unit in near-wall turbulence", J. Fluid Mech., Vol. 213, pp. 225.

Kim, J., Moin, P. and Moser, R., 1987, "Turbulent statistics in fully developed channel flow at low Reynolds number", J. Fluid Mech., Vol. 177, pp. 133.

Orlandi, P., 2000, "Fluid Flow Phenomena: A Numerical Toolkit", Kluwer academic publishers.

Piomelli, U., Yu, Y. and Adrian, R., 1996, "Subgrid-scale energy transfer and near-wall turbulence structure", Phys.

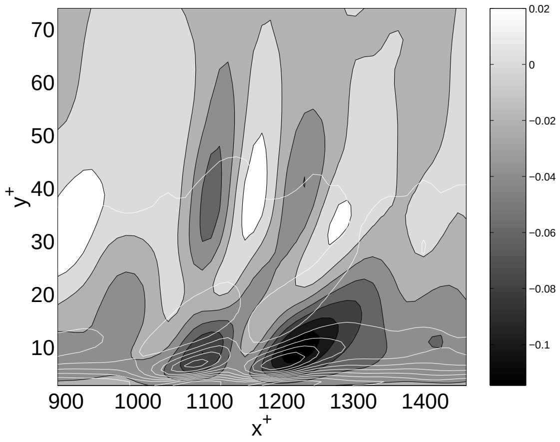

(a)

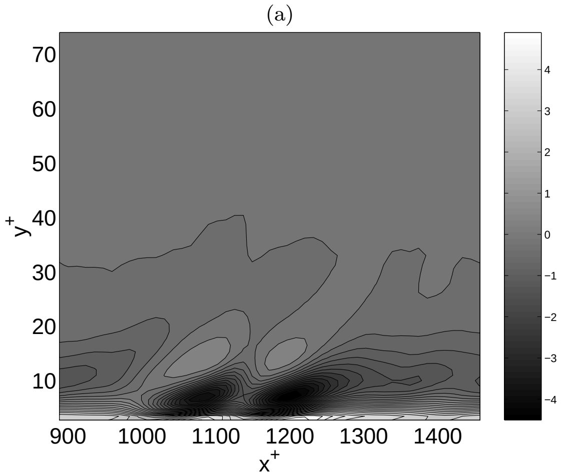

(b)

Figure 6: Forward scatter event of SGS energy dissipation detected at $y^+ \simeq 14$. (a) Map of Q-criterium and white contours of SGS enstrophy dissipation. (b) Map of SGS enstrophy dissipation. All values are in global units.

Fluids, Vol. 8, Num. 1, pp. 215.

Robinson, S. K., 1991, "The kinematics of turbulent boundary layer structure", Technical Memorandum TM-103859, Ames Research Center, Moffet Field, California.

Schlatter, P., Stolz, S. and Kleiser, L., 2005, "Evaluation of high-pass filtered eddy-viscosity models for large-eddy simulation of turbulent flows", Journal of Turbulence, Vol. 6, Num. 5, pp. 1.